Numerical Modelling of Bed Sorting and Armouring in Meandering Channels - Applications from the East Fork Lewis River - Ridgefield Pits Area, USA

Shuang Gao*[1], Mitchell Smith[1], Ian Teakle[1], Keith Marcoe[2] and Paul Kolp[2]

1 BMT Eastern Australia, Australia
2 The Lower Columbia Estuary Partnership, USA
* e-mail: shuang.gao@bmtglobal.com

Abstract

A multiple sediment fraction module was developed to predict bed morphological change with allowances for bed sorting and armouring. Meyer-Peter Müller's equation is applied to predict the scale of bedload for bed materials of different grain sizes. In order to assess the impact of bed sorting and armouring the model assumes that the river bed consists of two layers: (1) a surface exchange layer that can coarsen and regulate the supply of different sediment fractions based on the sediment composition; and (2) a sub-surface layer that supplies sediments as the surface layer is eroded. The model was validated against existing publications of lab-scale and field experiments. The modelled results show agreement with the experimental data, indicating the model is capable of predicting the morphological changes with the consideration of the sorting of bed materials. The model was then applied to estimate the potential for channel stability, including patterns of aggradation and degradation in a reach of the East Fork River, Oregon, USA.

Keywords: Numerical modelling, river morphology, bed sorting, bed armouring, TUFLOW FV

1 Introduction

Natural river bed materials typically consist of sediment mixtures comprising different grain sizes and sediment types. In a meandering river, coarse materials tend to exist near outer banks while finer sands and silts settle near the inner banks. Both bed armouring and sediment sorting play a key role in this redistribution of sediments. To reliably estimate sediment transport rates and long-term river morphology it is necessary that the underlying transport models include these processes.

Various sediment transport formulae have been developed to estimate the scale of suspended/bedload transports based on both experimental data and theoretical considerations (Meyer-Peter and Müller, 1948; Ashida and Mitchiue 1971; van Rijn 2007a, 2007b) and these formulae have been widely applied in numerical models. Ashida et al (1990) conducted a lab scale experiment to study bed sorting behavior in a meandering channel and applied a depth-averaged shallow water model to predict the bed morphology. Maeshima et al (2011) later carried out field experiments in a straight and curving channel, and applied a quasi-3D shallow water model to simulate the bed morphology under the influence of strong secondary currents. These well controlled experimental studies have also provided valuable verification data for developing numerical models to predict fluvial sediment transport and morphological processes.

With advancements in computational power 3D modelling has become increasingly efficient and accessible to examine complex river flow behavior. Here the 3D numerical engine TUFLOW FV is applied to model the hydrodynamics coupled with a sediment transport module resolving multiple sediment fractions in order to predict changes in bed morphology. The model is validated against the two experimental datasets of Ashida and Maeshima and then applied to real world case study to estimate the potential for channel stability, including patterns of aggradation and degradation, in a reach of the East Fork Lewis River, Washington USA.

2 Numerical Model

2.1 Hydraulic Model

TUFLOW FV is a finite volume numerical engine that solves the conservative integral form of the non-linear shallow water equations, including viscous flux terms and source terms (Guard et al, 2013). For the present application a three-dimensional approach using sigma-coordinates was adopted to consider the impact of secondary currents occurring in meandering channels. The standard k-ε closure in GOTM, a generic one-dimensional water column turbulence model (http://www.gotm.net), was employed for the parameterisation of vertical turbulent fluxes of momentum.

2.2 Bed Shear Stress

The bed shear stress predicted by the 3D hydraulic model is used to estimate the bedload transport rate and the suspended sediment concentration:

$$\tau_{bx} = \rho C_b u_b \sqrt{u_b^2 + v_b^2} \tag{1}$$

$$\tau_{by} = \rho C_b v_b \sqrt{u_b^2 + v_b^2} \tag{2}$$

where, τ_{bx} and τ_{by} are the bed shear stress in the Cartesian x and y direction, ρ is the density of water, u_b and v_b are the velocity at the bottom cells, and C_b is the bottom drag coefficient calculated using a roughness-length relationship:

$$C_b = \left(\frac{\kappa}{ln(30z'/k_s)}\right)^2 \tag{3}$$

where, κ is the von Karman's constant, z' is the height of the bottom cell above the bed level, and k_s is the effective bed roughness length.

2.3 Bedload

The bedload transport rate along the direction of the bed shear stress is estimated using the Meyer-Peter and Müller equation:

$$\Phi = \frac{q_b}{\left[g(s-1)d^2\right]^{1/2}} = 8(\tau_* - \tau_{*c})^{1/2} \tag{4}$$

where, Φ is the dimensionless bedload transport rate, q_b is the bedload transport rate per unit width, g is the gravity acceleration, s is the ratio of densities of sediment and water, d is the representative grain size, τ_* is the Shields parameter and the τ_{*c} is the critical value of τ_* at threshold of motion:

$$\tau_* = \frac{\tau_b}{g\rho(s-1)d} \tag{5}$$

This study also employed Shimizu et al (1995)'s method to consider the impact of bed slope on the direction of bedload transport. The bedload components in the direction of the bed shear stress $\hat{s}$ and perpendicular to the direction of the bed shear stress $\hat{n}$ have the following relationship:

$$\Phi = \sqrt{\Phi_{\hat{s}}^2 + \Phi_{\hat{n}}^2} \tag{6}$$

with

$$\frac{\Phi_{\hat{s}}}{\Phi_{\hat{n}}} = -\sqrt{\frac{\tau_{*c}}{\mu_s \mu_k \tau_*}} \frac{\partial z}{\partial \hat{n}} \tag{7}$$

where, μ_s and μ_k are the static and kinetic friction coefficient (assumed as 0.6 and 0.48, respectively) and $\partial z/\partial \hat{n}$ is the bed slope component perpendicular to bed shear stress direction.

2.4 Suspended Load

The suspended load transport rate is modelled using a standard 3D mass conservation equation, with a sediment pickup rate of:

$$E = w_s C_a \tag{8}$$

where, w_s is the settling velocity, and C_a is the reference concentration close to the bed given by (van Rijn 2007b).

2.5 Bed Sorting and Armouring

To assess the impact of the bed sorting and armouring the model assumes that the river bed consists of two layers: (1) a surface exchange layer that can coarsen and regulate the supply of different sediment fractions based on the sediment composition; and (2) a sub-surface layer that supplies sediments as the surface layer is eroded (Figure 1). This idea is similar to Ashida et al (1990)'s exchange layer method and the Active Layer Mixing Method used in HEC-RAS (Brunner, 2016).

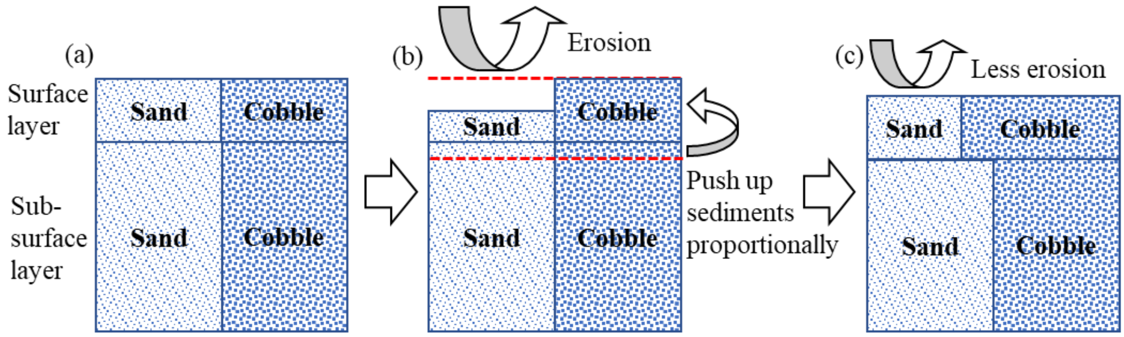

Figure 1. An illustration of bed armouring process. (a) The surface layer consists of 50% of sands and 50% of cobbles initially; (b) As the finer fraction is eroded, the sub-surface layer sediments are pushed up to the surface layer proportionally to the sediment composition; (3) The surface layer coarsens and regulates the supply of erodible fine sediment.

A discrete number of sediment fractions can be used to represent the bed material size distribution. The bedload transport rates and pickup rates are calculated for each fraction using equations (6) ~ (8), and adjusted proportionally based on the volumetric portion at the surface exchange layer $V_{s,i}$:

$$\Phi_i' = \Phi_i \frac{V_{s,i}}{\sum V_{s,i}} \tag{9}$$

$$E_i' = E_i \frac{V_{s,i}}{\sum V_{s,i}} \tag{10}$$

where, Φ_i and E_i are the dimensionless bedload transport rate and pickup rate calculated by equations (6) and (8) for each fraction assuming the bed is completely filled by one sediment fraction, while Φ_i' and E_i' are those rates considering the supply of different sediment fractions based on the bed sediment composition.

Finally, the bed elevation z_b is changed based on the following equation:

$$(1-\lambda)\rho_s \frac{\partial z_b}{\partial t} + \frac{\partial \sum q_{bi,x}'}{\partial x} + \frac{\partial \sum q_{bi,y}'}{\partial y} + \Sigma(w_{si}C_{bi} - E_i') = 0 \tag{11}$$

where, λ is the bed layer porosity, ρ_s is the density of bed material and C_b is the sediment concentration at the bottom cell.

3 Model Verifications

3.1 Experiments

The sediment model was validated by comparing modelling results with two published experiments. Ashida et al (1990) conducted a lab-scale experiment of a meandering channel with bed material ranging from d_{10}=0.5mm to d_{90}=4mm. The experiment was started with a flat channel bed and was run until the bed form reached steady state conditions. Maeshima et al (2011) carried out a field-scale experiment in a straight and meandering channel with a trapezoidal cross section using a bed material distribution closer to gravel-bed rivers (d_{10}=1mm ~ d_{90}=200mm). A low flow of 2.0 m^3/s was applied to form an initial bed elevation and material distribution and higher flows were applied consecutively. The bed elevation was recorded between each run. The experimental conditions are summarised in

Table 1, the scales of the experimental flumes are illustrated in Figure 2, and the sediment size distributions are presented in Figure 3.

Table 1. Summary of experimental and field conditions.

Study	Case	Flow Rate (l/s)	Depth (cm)	Median Grain Size (mm)	Cell Size (m)
Ashida et al (1990)	A1	1.2	1.65	1.74	0.03 * 0.02
	A2	3.6	4.26	1.74	0.03 * 0.02
Maeshima et al (2011)	M1	2.0	0.34	50	0.5 * 0.25
	M2	3.2	0.56	50	0.5 * 0.25
	M3	8.0	0.80	50	0.5 * 0.25
East Fork Lewis River	E1	141.6		50	5~10
	E2	588.9		50	5~10

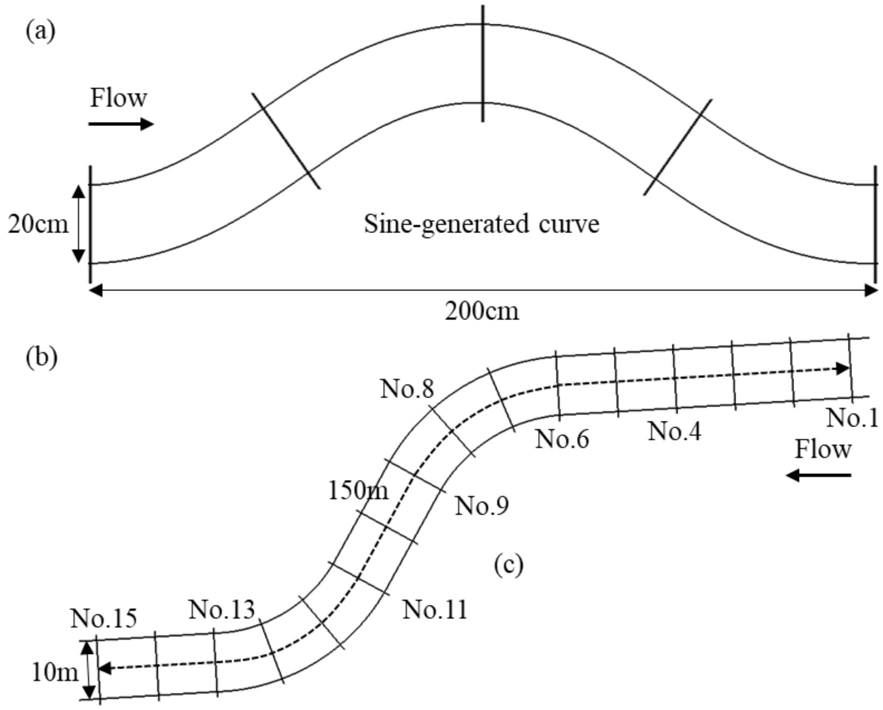

Figure 2. Experimental channels of (a) Ashida et al (1990) and (b)Maeshima et al (2011)

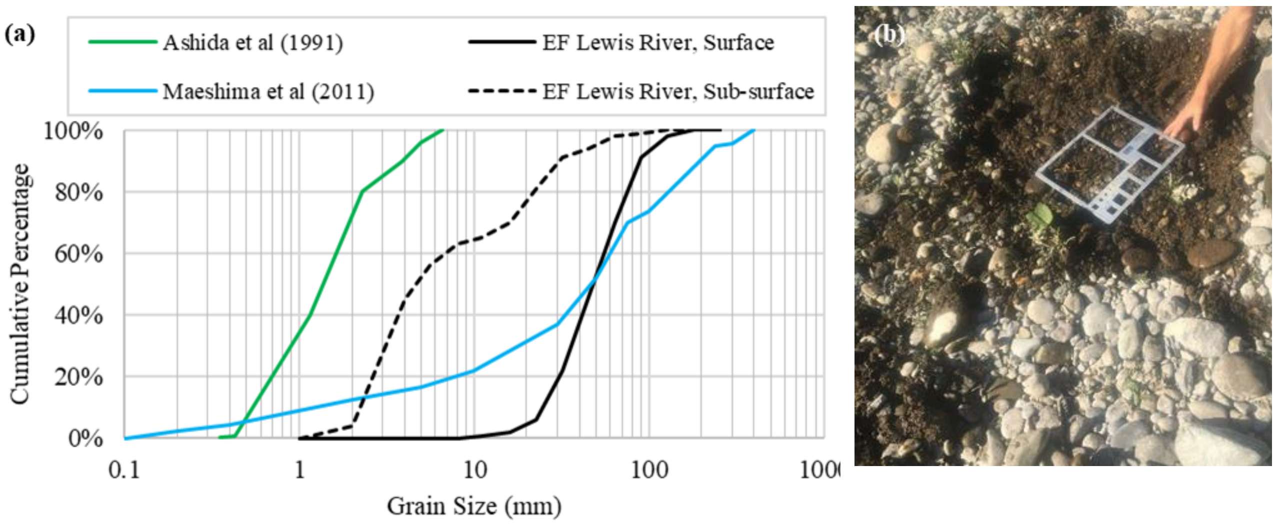

Figure 3. (a) Sediment size distributions of the experimental and field studies. (b) Typical surface and sub-surface layer of the East Fork Lewis River bed material.

For both model validations bed material was represented via a discrete number of sediment fractions based on reported particle size distributions (refer Table 2). The modelled bed roughness length k_s was first calibrated to reproduce the water depths/levels reported in the experiments and was then applied to the sediment transport calculations (Equation 3). Soulsby (1997)'s formula was used to estimate the critical Shields parameters τ_{*c} for the median grain size, and the Egiazaroff's method (as described in van Rijn 2007c) was used to determine τ_{*c} for each grain size. The thickness of the surface exchange layer was specified to be equivalent to the global d_{90}. For Maeshima et al (2011)'s experiments an idealised initial cross section was applied throughout the channel due to the lack of initial bed elevation data.

Table 2. Representative sediment sizes used in the simulations

	Ashida et al (1990)				
Representative Size (mm)	0.7	1.3	1.74	2.5	4
Size Distribution (mm)	< 1.1	1.1 - 1.5	1.5 - 2.0	2.5 - 3.0	> 3.0
	Maeshima et al (2011)				
Representative Size (mm)	2	10	50	100	200
Size Distribution (mm)	< 6	6 - 25	25 - 75	75 - 150	> 150
	EF Lewis River				
Representative Size (mm)	2	25	50	100	-
Size Distribution (mm)	< 8	8 - 32	32 - 64	64 - 256	-

3.2 Experimental Results Comparison to Ashida et al (1990)

Figure 4 and Figure 5 provide the measured and simulated results of bed elevation change for Cases A1 and A2. Case A1's flowrate of 1.2 l/s results in peak bed shear stresses only slightly exceeding the critical shear stresses of the bed materials (0.8~2.0 N/m^2). Case A2 with a higher flowrate of 3.6 l/s results in stress of 1.6~6.2 N/m^2, which are well above the critical values resulting in widespread sediment movement and bed response. The model reproduced the locations of the maximum erosion (near Φ=90° and 270°) and deposition (at Φ=0° ~ 90° and 180° ~ 270°) in Case A1. However, the maximum erosion depth was underestimated, and the maximum deposition depth was overestimated. This could be attributed to the accuracy of the empirical bedload formula near the threshold of motion. On the other hand, the magnitudes of the erosion and deposition were well predicted in Case A2, however, the position of maximum erosion occurred slightly downstream compared with the experiment. This may indicate that the induced helical flow circulation is not sufficiently strong in the model, however without velocity measurements this hypothesis could not be directly tested.

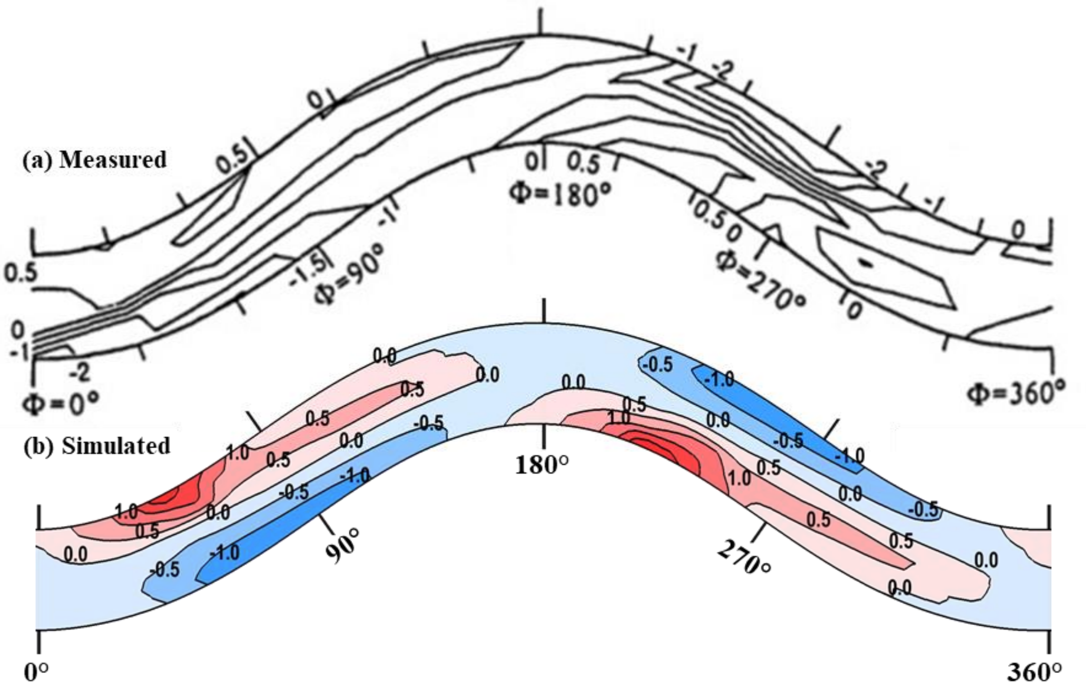

Figure 4. Measured and simulated bed elevation changes of Ashida et al (1990)'s experiment Case A1. (a) Measured; (b) Simulated.

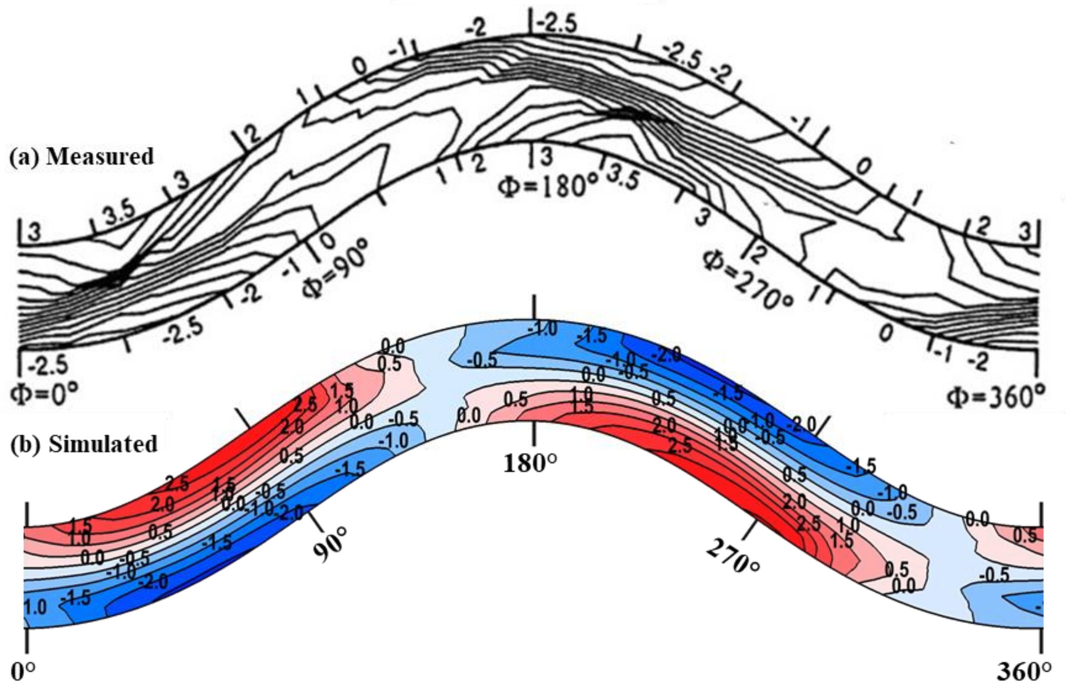

Figure 5. Measured and simulated bed elevation changes of Ashida et al (1990)'s experiment Case A2. (a) Measured; (b) Simulated.

3.3 Experimental Results Comparison to Maeshima et al (2011)

Figure 6 presents the measured and simulated change in bed elevation results immediately prior and following Case M3. Significant erosion along the outer bank of the curved section and deposition along the inner bank are observed in the measurements (from cross section 6 to 9). The magnitudes of the erosion and deposition are well modelled, however, the location of erosion/deposition occurs slightly downstream compared to that measured (from cross section 8 to 11). Similar to the previous section this may in part be due to under-prediction of the strength of the helical flow circulation, but may also be due to the fact that the right/left bank were not at even elevations in the experiment (please refer to the Figure of Maeshima et al, 2011). Figure 7 compares the absolute bed elevation at cross sections 4 and 8. At cross section 4, some slumping occurs as the bank is eroded and deposited into the main channel. At cross section 8, the outer bank is eroded, and the sediment deposited at the inner bank. These phenomena were generally well reproduced by the model and are typical of sediment sorting and redistribution at bends.

The verifications of both experiments indicate that the location of erosion/deposition occurs slightly downstream in the simulations compared to the experiments. As neither of the experiments has enough hydraulic data to evaluate the development of the helical flow circulation, more tests are required to improve the capability of secondary current simulation, e.g. testing different horizontal and version turbulence models.

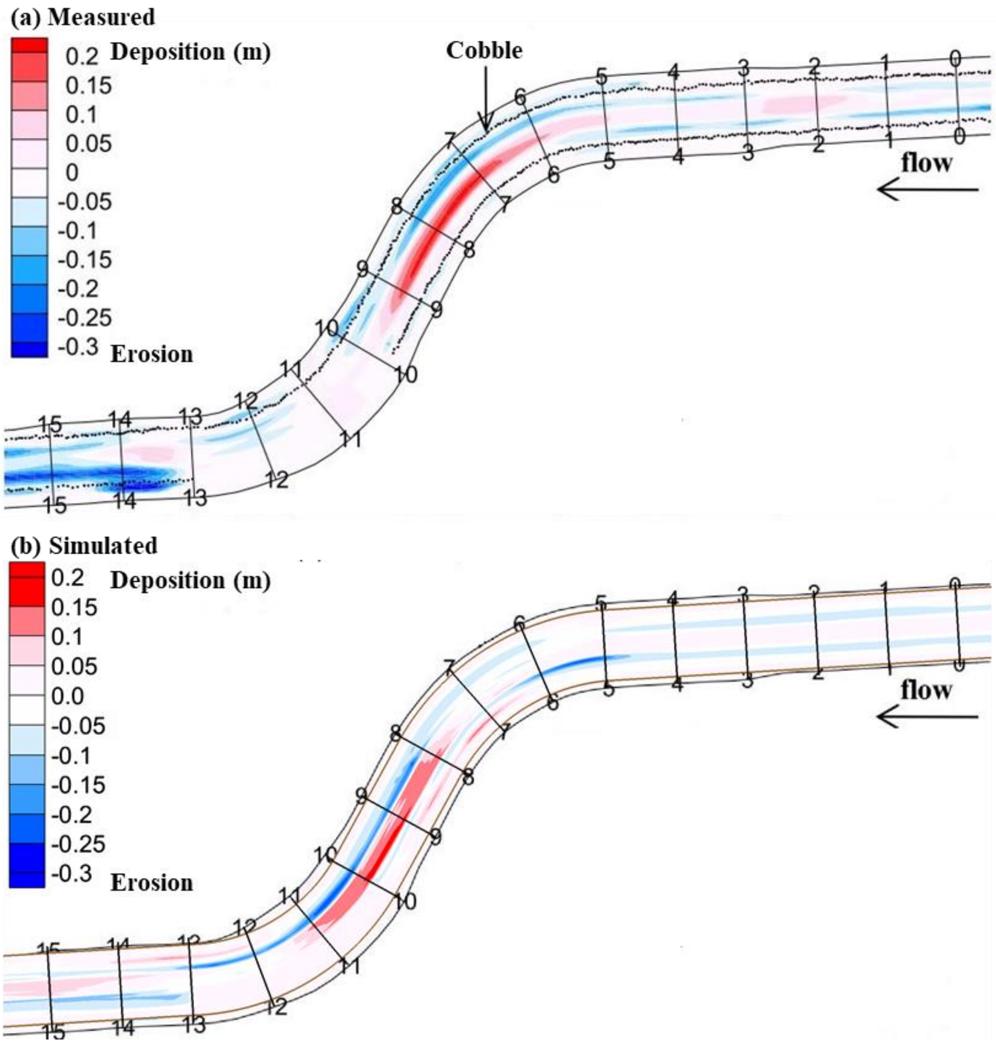

Figure 6. Measured and simulated bed elevation changes before and after run M3 of Maeshima et al (2011)'s experiments. (a) Measured; (b) Simulated.

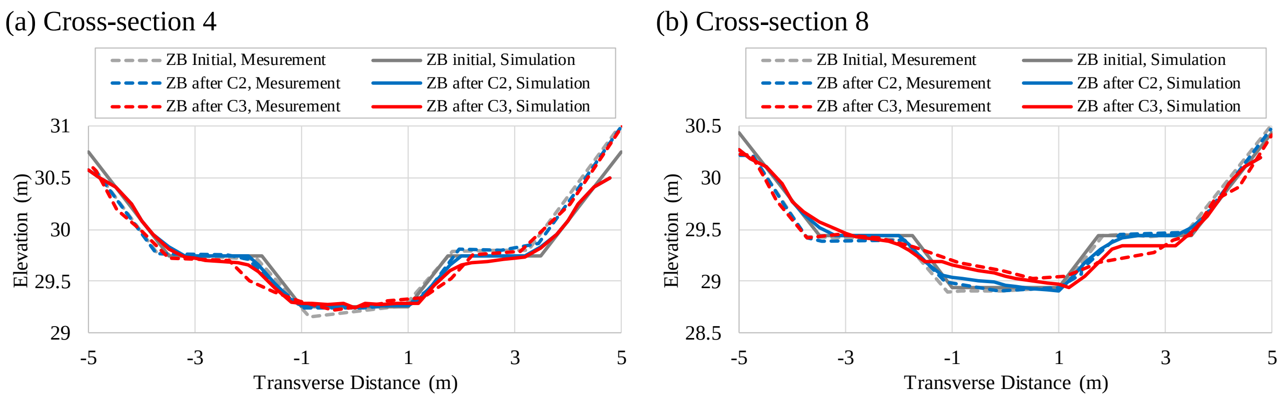

Figure 7. Measured and simulated bed elevation at cross sections 4 and 8.

4 Case Study East Fork River - Ridgefield Pits Study Area

4.1 Study Area

Following validation the model was used to infer channel stability, including patterns of aggradation and degradation in a reach of the East Fork Lewis River - Ridgefield Pits Area. The channel in this region has a critical influence on the life histories of salmonids throughout the catchment. Historic gravel mining activities in the area have created deep floodplain lakes (Figure 8a). Following cessation of mining the main river channel avulsed into the nine abandoned gravel pits during the 1996 flood. The modified regime has created deep and cold ponds along the main river course which are unfavorable to the migration of salmonids, forming a barrier to upstream spawning habitats. Since 1996 the river has been highly dynamic, changing course frequently as can be seen from the historical flow paths of the river (Figure 8b). Field sediment survey of the study area indicated a distinct in-channel surface armour layer consisting of material size of 15 ~ 200mm with a finer sub-surface layer of much wider sediment distribution range (Figure 3). Therefore, it is expected that bed sorting/amouring has a significant influence on the river morphological response and thus was an excellent case study to assess the performance of the new bed armouring routines.

The Ridgefield Pits model domain is bounded by the black dashed polygon in Figure 8b. Bathymetric/topographic data collected in 2017 was applied as the initial bed elevation. Aerial photography and sediment data were used to estimate an initial bed sediment distribution. To improve this sediment distribution a constant flowrate of 140m^3/s (or 5000cfs) was applied for an extended period to allow the formation of an initial equilibrium bed armour layer. The selection of this flowrate followed review of historical flow data, aerial photography and model predicted bed shear stresses and was sufficient to transport and redistribute fine sediments whilst not being large enough to mobilise armour material. Following bed warmup the December 2015 (588.9 m^3/s or 20800 ft^3/s peak flow rate) was modelled and comprises the largest complete hydrograph from the available record. The sediment fractions used in the modelling are summarised in Table 2. Sediment entering and exiting the model was assumed to be identical to that adjacent to the model boundary, a so-called zero-gradient boundary.

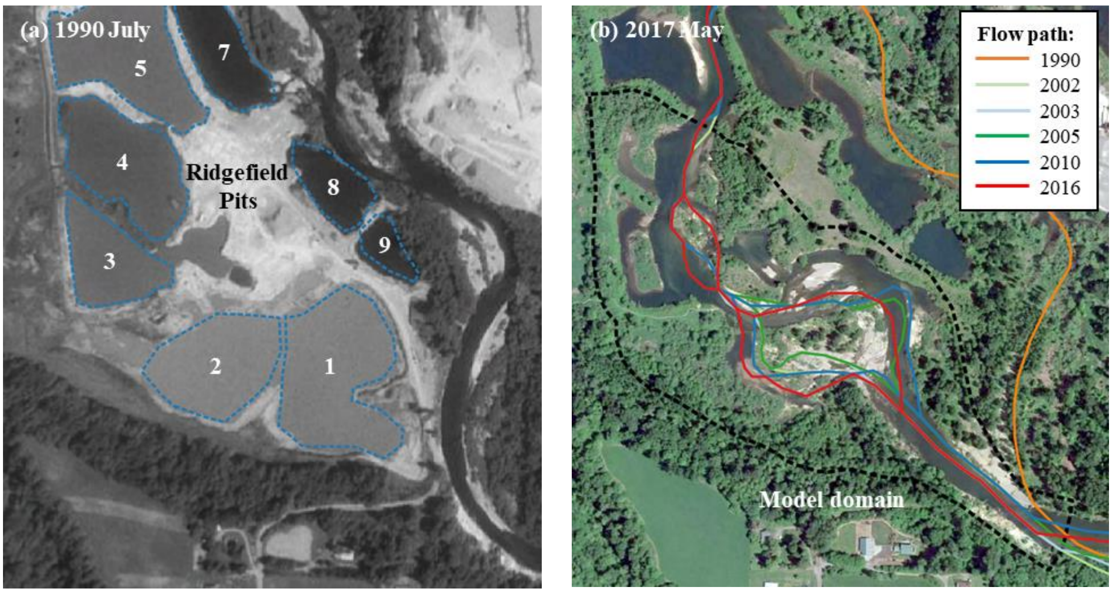

Figure 8. Google aerial images of the Ridgefield Pits area in (a) 1990 and (b) 2017.

4.2 Simulation results and discussions

Figure 9a shows the flood hydrograph of the December 2015 event, while Figure 9b~9d present a snapshot of bed elevation changes before, during and after the flood peak. Before the peak (Figure 9b), the model predicts degradation near the outer bank of the bend and at the entrances of the small avulsion channel (highlighted by the white arrows). At the flood peak (Figure 9c), the straight section upstream of the bend was eroded significantly, and the eroded sediments moved downstream. After the flood (Figure 9d), these sediments eventually settle at the entrance of the bend and in the location of the old Pit 1 and 2 (refer Figure 8a). In general, degradation is expected to happen at the outer bank of the bend and at the entrance of the avulsion channel after such a flood event, and aggradation is expected at the entrance of the bend inside the pits. This is consistent with the trend observed from the Google aerial imagery (Figure 10). The model result also implies that the morphological change in an actual flood event is a dynamic process unlike the experiments, where near steady-state bed morphology was attained under steady flow conditions. Therefore, it is crucial to conduct more field scale simulations under different flow rates and durations in order to understand the long-term channel stability.

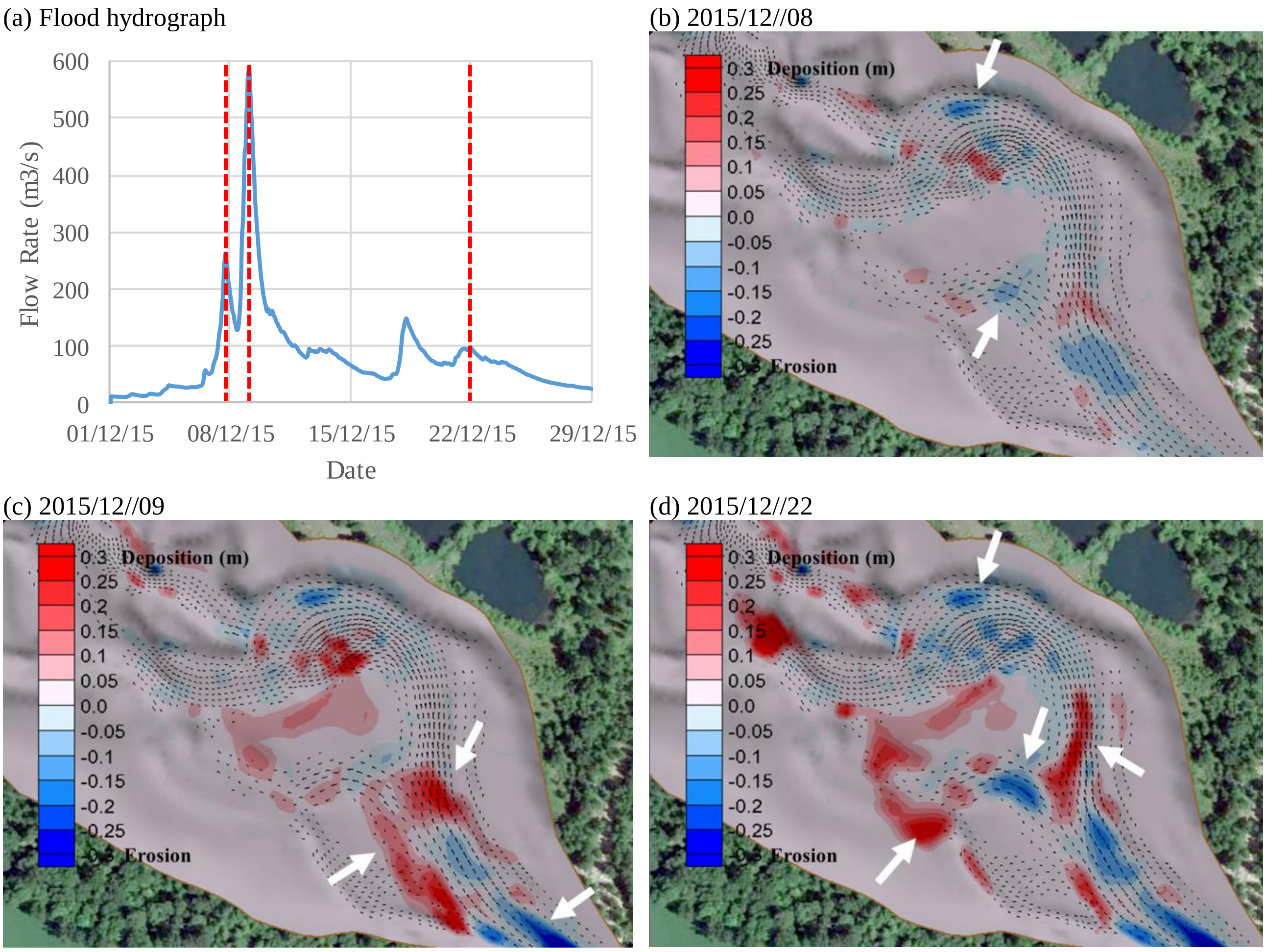

Figure 9. East Fork Lewis River simulation. (a) Flood hydrograph, and the simulated bed elevation changes (b) before the flood peak, (c) during the flood peak, and (d) after the flood.

Figure 10. Google areal images of the modelling area before and after the 2015 flood. (a) 2014 dry season; and (b) 2016 dry season.

5 Conclusions and Future Studies

A multiple sediment fraction module was developed for the 3D numerical engine TUFLOW FV to predict bed morphological change with allowances for bed sorting and armouring. The modelling results showed agreement with two existing publications of lab-scale and field experiments. The model also demonstrated capability to estimate the potential for channel stability, including patterns of aggradation and degradation in a real-world gravel river.

Recommendations arising from the research and testing are:

- The accuracy of a hydrodynamic model to predict the development of helical flow circulations in meandering channels is fundamental to accurately predicting morphological evolution. Therefore, model validation against detailed measurements of the velocity fields created by helical flow circulations would be highly beneficial.
- The morphological change in an actual flood event is a dynamic and non-steady-state process. Models would benefit from validation against dynamic flow field experiments or field data.
- Field scale simulations under different flow rates and durations would be beneficial to understand long-term channel stability and further assist with model validation.

References

[1] Meyer-Peter, E. and Müller, R. (1948): "Formulas for bed-load transport". Proceedings of 2nd meeting of the International Association for Hydraulic Structures Research, Stockholm, 39-64.

[2] Ashida, K. and Michiue, M. (1971): "Studies on bed load transportation for nonuniform sediment and river bed variation". Disaster Prevention Research Institute Annuals, Kyoto University, No. 14 B, 259-273. (in Japanese)

[3] Van Rijn, L., C. (2007a): "Unified view of sediment transport by currents and waves. I: Initiation of motion, bed roughness and bed load transport". Journal of Hydraulic Engineering ASCE, Vol. 133, No. 6, 649-667.

[4] Van Rijn, L., C. (2007b): "Unified view of sediment transport by currents and waves. II: Suspended transport". Journal of Hydraulic Engineering ASCE, Vol. 133, No. 7, 668-689.

[5] Ashida, K., Egashira, S., Liu, B., and Umemoto M. (1990): "Sorting and bed topography in meander channels". Disaster Prevention Research Institute Annuals, Kyoto University, No. 33 B-2, 261-279. (in Japanese)

[6] Maeshima, T., Iwasa, M., Osada, K., and Fukuoka, S. (2011): "Study of river-bed variation and its grain size distribution in compound stony-bed river with meandering and straight channel"., Proceedings of Hydraulic Engineering, JSCE, Vol. 55. (in Japanese)

[7] Guard, P., Nielsen, C., Ryan, P. Teakle, I., Moriya, N. and Kobayashi, T. (2013): "Parameter sensitivity of a 2D finite volume hydrodynamic model and its application to tsunami simulation". Proceedings of 2013 IAHR Congress, Beijing, China.

[8] Shimizu, Y., Watanabe, Y. and Toyabe, T. (1995): "Finite amplitude bed topography in straight and meandering rivers". JSCE Journal of Hydraulic, Coastal and Environmental Engineering, No. 509/II-30, 67-78. (in Japanese)

[9] Brunner, G., W. (2016): "HEC-RAS, river analysis system hydraulic reference manual". US Army Corps of Engineers.

[10] Van Rijn, L., C. (2007c): "Unified view of sediment transport by currents and waves. III: Graded beds", Journal of Hydraulic Engineering ASCE, Vol. 133, No. 7, 761-775.

Errata

Page 2, Equation (7): replace $\frac{\Phi_{\hat{s}}}{\Phi_{\hat{n}}}$ by $\frac{\Phi_{\hat{n}}}{\Phi_{\hat{s}}}$

Page 4, Table 1: the unit of the flow rates for East Fork Lewis River models are m^3/s, not l/s

Page 7, Figure 7: replace “C2” and “C3” by “M2” and “M3”, respectively